Study on FPGA-Based Real-Time Signal Processing for SOI MOSFET Single-Photon Detector

学 位 論 文 要 約

Summary of Doctoral Thesis

専　　攻：　ナノビジョン工学　　氏　名：マニバンナン レバティ
Course：　Nanovision Technology　　Name：Manivannan Revathi

論文題目：SOI MOSFET 単一フォトン検出器のための FPGA に基づく実時間信号処理の研究
Title of　Thesis：Study on FPGA-Based Real-Time Signal Processing for SOI MOSFET Single-Photon Detector

論文要約：
Summary：

Introduction

Single-photon detectors are extensively used in the field of fluorescence measurement,[1),2)] light detection and ranging (LiDAR),[3)] scintillation measurement,[4)] quantum cryptography,[5)-7)] optical time domain reflectometer,[8)] fluorescence lifetime imaging (FLIM),[9),10)] and so on. Such applications require some of the combined following properties such as large maximum count rate (MCR), small dark count rate (DCR), high quantum efficiency (QE), wide spectral response, high timing resolution, high photon number resolution (PNR), etc., and continual efforts have been made to improve such properties. One fundamental approach for the improvement is to directly count photogenerated elementary charges (electrons or holes) by highly sensitive electrometers such as single-electron transistors (SET)[11)] and scaled-down FETs.[12)] The SET-based approach includes the photodetector by A. N. Cleland, et al.,[13)] the quantum dot (QD) detectors[14),15)] and the tunnel-junction-array detector,[16)] and the FET-based one includes the QD-gated FET,[17),18)] the Si-nanowire detector,[19),20)] the charge-sensitive infrared phototransistor (CSIP)[21),22)] and QD optically gated FET (QDOGFET).[23),24)] Such detectors feature wide coverage of the spectrum range from submillimeter waves to visible lights, small DCR, excellent PNR, and low-voltage operation in contrast to the ordinary single-photon detectors such as avalanche photodiodes (APDs)[25)] and photomultiplier tubes (PMTs)[26)] that require high voltages for charge multiplication. However, these SET or FET-based single-photon detectors show the complex output waveforms consisting of rising and falling edges corresponding to photogeneration and spontaneous recombination of charges, and multiple signal levels reflecting the amount of accumulated charges, and therefore the dedicated signal processing is required especially when the lifetime of the charged state is comparable to the photon incident interval.

In order to address this issue, a signal processing algorithm is developed this time and implemented to field programmable gate array (FPGA) for the real-time usage. Silicon-on-insulator (SOI) MOSFET single-electron detector[27),28)] is used to demonstrate the proper operation of the processor by verifying the statistical distribution of the photogenerated holes that follows the Poisson distribution.

To the best of our knowledge, this is the first time to implement the signal processing algorithm dedicated to the photon detectors based on elementary charge counting to FPGA, and to verify its proper operation based on photon number statistics, which is scientifically meaningful in view of the potentials of such a class of detectors with wide spectral coverage, small DCR, excellent PNR and low-voltage operation.

Device structure and experimental methods

Figure 1 shows the basic structure of single-photon detector. It has dual-gate structure consisting of a short lower gate (LG) and a long upper gate (UG). The dual-gate structure is adopted to electrically create a narrow potential well for storing the photogenerated holes. The narrow well is manifested by the better immunity to the short channel effect, i.e. shorter LG can be used without losing drain current

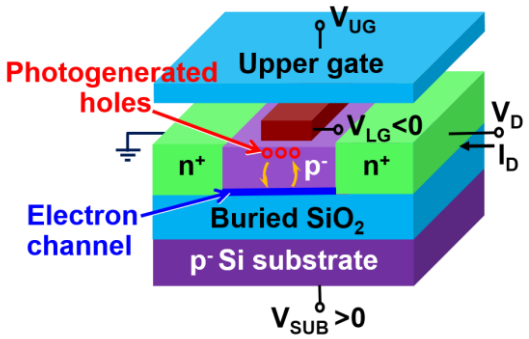

Fig. 1. Cross-sectional view of the SOI MOSFET single-photon detector. In this study, a device with L=70 nm and W=110 nm is used. The thicknesses of the buried oxide, SOI, LG oxide and insulator below the UG are 145, 50, 5 and 440 nm respectively.

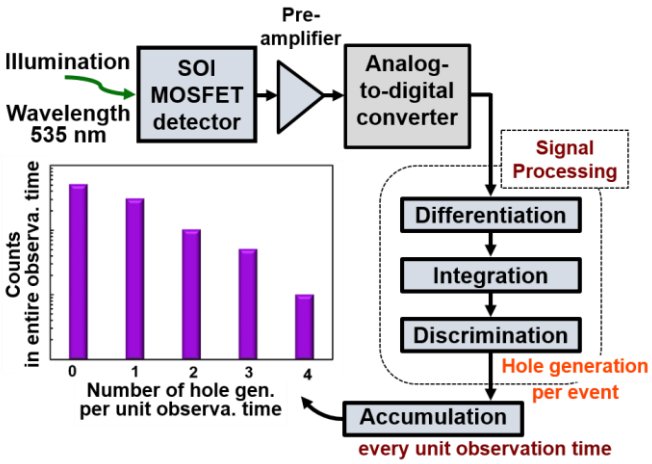

Fig. 2. Block diagram of the measurement setup to obtain photon number statistics for SOI MOSFET single-photon detector.

Table I. Specification of the signal processing system including the preamplifier. The future target[30] assumes the replacement of PMT in such an application as microplate readers[31] for luminescence observation[32].

Parameter	This study	Future target
Preamplifier sensitivity	10^{10} V/A [a]	1.8×10^{6} V/A
Preamplifier bandwidth	800 Hz [a]	13 MHz
ADC resolution	12 bit	
Sampling frequency	38.5 kHz	38.5 MHz
FPGA clock frequency [b]	256 kHz	256 MHz

[a] DL Instruments model 1211 [b] Xilinx Zynq ZC702

controllability[29], and results in higher sensitivity to a hole, compare to the case with the single-gate structure[28]. The thicknesses of buried oxide, SOI, LG oxide and pre-metal dielectrics are 145, 50, 5 and 440 nm, respectively. In this study, a device with a LG length of 70 nm and a channel width of 110 nm is tested. Since the shorter LG gives a better sensitivity to the presence of photogenerated holes, the shortest LG by the available process technology is selected. Photogenerated holes are stored below the LG when positive and negative voltages are applied to the substrate and LG, respectively. The presence of holes is detected as the increase in the current flowing through the back-side channel.

The photon counting method implemented in the signal processing unit is shown in Fig. 2, and Table I summarizes the specification of the signal processing system including the preamplifier. The future target[30] assumes the replacement of PMT in such an application as microplate readers[31] for luminescence observation[32], where typical MCR and the dynamic range[33] are 5 Ms^{-1} and 100 dB that could be improved to 170 dB at least by the use of the photon detectors based on elementary charge counting due to the reduced DCR. In this study, SOI MOSFET detector is subjected to light source with a wavelength of 535 nm at 300 K, and the drain voltage V_D is kept at 50 mV. The drain current is amplified by the current preamplifier (DL Instruments, model 1211) by a factor of 10^{10} V/A with a current suppression of 10^{-9} A to cancel the drain current (~10^{-9} A) and make the output level nearly equal to zero. The amplified output is delivered to the analog-to-digital converter (ADC) of Zynq ZC702 FPGA board by Xilinx. To detect the events of hole generation by photon incidence, the digitized output is processed by signal processing algorithm, where the differentiation and integration operations are performed sequentially. The differentiation is based on the quadratic fitting to three data points and the calculation of the first derivative, [34] which makes the processing insensitive to the baseline shift. Further, the differentiated signal is integrated if the peak value exceeds the threshold level, which makes the processing immune to the noise. The integration time is nearly equal to the rise time of the input pulses that is about 250 μs for the preamplifier bandwidth of 800 Hz. Finally, the integrated signal is discriminated to judge the number of photogenerated holes. We adopted the FPGA to realize the fast processing. However, as shown in the column "this study" of Table I, the sampling and FPGA clock frequencies are set rather low corresponding to the narrow bandwidth of the preamplifier. According to the MATLAB simulation[35], the

data stream at a sampling frequency of 38.5 kHz (test condition in this study, see Table I) can be processed in 20% of the real time, but if it exceeds 500 kHz, real-time processing is not possible. Since the FPGA clock frequency can be increased up to 250 MHz, the processing at a sampling frequency close to 40 MHz can be realized, which ensures the wide usage of single-photon detectors based on elementary charge counting. If the detectors with higher output current are selected to be compatible with the preamplifier sensitivity in the column "future target" of Table I, the issue of the narrow bandwidth (800 Hz in this study) of the preamplifier can be resolved, and we are able to make full use of the high sampling frequency and improve the MCR.

In order to verify the proper operation of the signal processor, the statistical variation of photogenerated holes is studied. The hole numbers are accumulated in a unit observation time T, and then the bin counter corresponding to the accumulated number is incremented by one after every T. Histogram of the number of holes generated in a T is made after the entire observation time (T_{total}). In order to observe the evolution of the histogram, light intensity is varied from 1.21 to 9.75 μW/cm^2 for T's of 8.32 and 33.28 ms, which results in the variation in the average number of hole generation λ from 0.038 to 1.354 holes in T.

Results and discussion

The signal waveform at each stage is shown in Fig. 3. The digitized detector output and the corresponding differentiated signal are shown. The differentiated signal above the threshold level is integrated, and then discriminated to determine the hole generation per event, which is shown as a triangular symbol. The right vertical axis indicates the number of photogenerated holes in the event. The SOI MOSFET single-photon detector together with this signal processor can resolve the photon number even if multiple photons enter at the same time. The hole generation rate plotted against the intensity of the incident light is shown in Fig. 4. The linear relationship suggests that the proposed signal processing algorithm can properly extract the hole generation information in real time. Based on the slope of the line

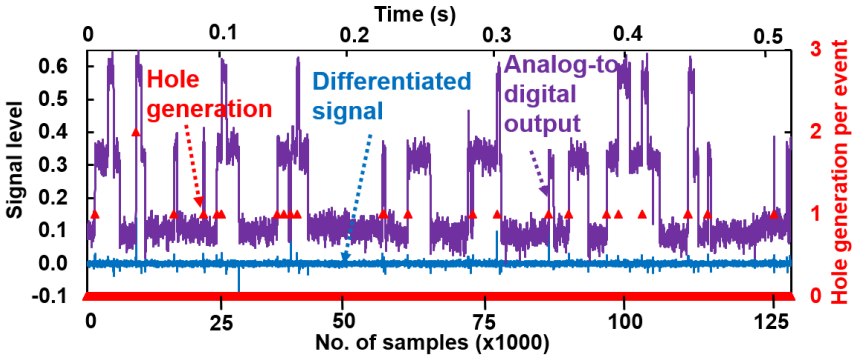

Fig. 3. Signal waveforms at different stages of the processing for the signal obtained under the illumination at the wavelength of 535 nm and the light intensity of 4.5 x 10^{-6} W/cm^2. The sampling frequency is 38.5 kHz corresponding to the narrow bandwidth (800 Hz) of the preamplifier. The unit observation time T for statistical analysis (8.32 or 33.28 ms in the current study) can be arbitrarily set as long as it is sufficiently longer than the sampling period.

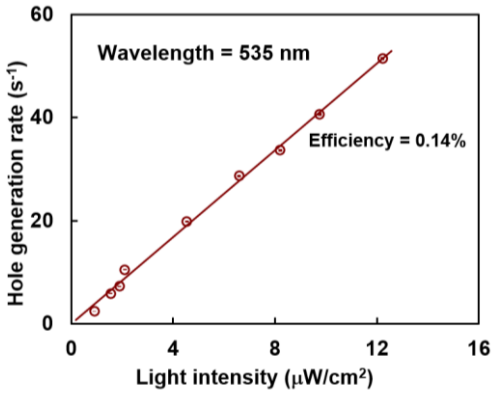

Fig. 4. Hole generation rate vs. light intensity. Solid symbols are measured data and solid curve is fitted line.

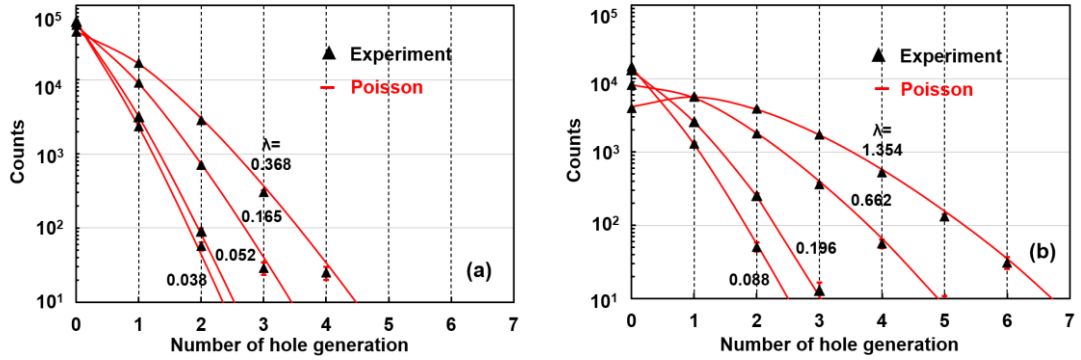

Fig. 5. Hole count distribution for different light intensities. λ represents the average number of hole generation in a unit observation times T of (a) 8.32 and (b) 33.28 ms. Solid lines represent the theoretical Poisson distribution. λ's of 0.038, 0.052, 0.165 and 0.368 in (a), and 0.088, 0.196, 0.662 and 1.354 in (b) correspond to the light intensity of 1.21, 1.54, 4.53 and 9.75 μW/cm^2, respectively.

in Fig. 4 and the detector active area of 1.07 μm × 0.11 μm, the nominal quantum efficiency (QE) is calculated to be 0.14%. The low QE is caused by the opaque UG, and could be improved by replacing the UG with a transparent one and/or introducing the optical antenna.[36] Based on the absorption coefficient of light (7.7×10^3 cm^{-1})[37] in Si at a wavelength of 535 nm, absorption in 50-nm-thick Si layer is estimated to be 3.8% without considering the surface and internal reflections. The similar discrepancy between the estimated absorption and the measured QE was reported before[27], and could be explained by the presence of the opaque UG.

Figure 5 shows the histogram of the counts in bins corresponding to the number of generated holes in a unit observation time T. For the T of 8.32 ms, the light intensities of 1.21, 1.54, 4.53 and 9.75 μW/cm^2 result in the average number of hole generation (λ) of 0.038, 0.052, 0.165 and 0.368, respectively, as indicated in Fig. 5 (a). Since the total observation time T_{total} is 532.48 s, the total counts are T_{total}/T = 64,000. To cover the wide range of λ, the T is further increased to 33.28 ms. In Fig. 5 (b), the λ values are increased fourfold for the same set of light intensities while the total counts are 16,000. As the λ increases, the counts for larger numbers of hole generation increase. The filled triangles are the number of counts obtained experimentally, and the solid lines are the theoretical Poisson distributions. The experimental

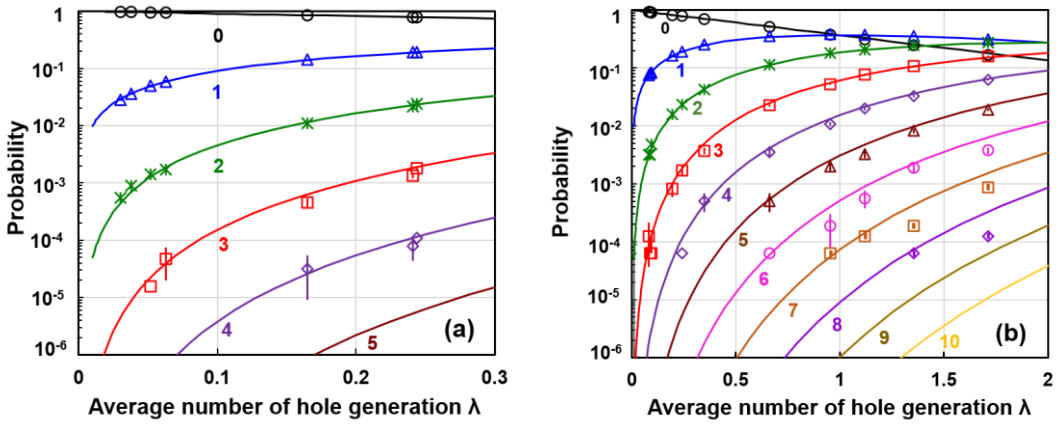

Fig. 6. Event probability corresponding to different numbers of hole generation in a unit observation time as a function of λ for unit observation times of (a) 8.32 and (b) 33.28 ms. Solid lines represents the theoretical Poisson distribution.

data coincide well with the theoretical ones within the error bar for all the levels of light intensity, suggesting that the observed hole generation follows the Poisson statistics as expected.

Figure 6 shows the event probability as a function of average number of hole generation λ for the unit observation time T of (a) 8.32 and (b) 33.28 ms. The probabilities are plotted against the λ by varying the light intensities. It also shows the theoretical curves based on Poisson distribution[エラー! 参照元が見つかりません。], i.e. the probability that a certain event takes place k times in a unit time is expressed by

$$P\,(N = k) = \frac{e^{-\lambda} \times \lambda^{k}}{k!}, \qquad (1)$$

where λ is the average event number (a positive real number), k is a natural number including zero, and $k!$ is the factorial of k. For instance, the probability to obtain k photons in an observation time T is given by equation (1) with $\lambda = RT$, where R is the incident rate [1/s] of photons. In Fig. 6, the numbers 0,1,2 and so on represent the number of hole generation in T, and the error bars are the square root of the experimental counts. The experimental data match the theoretical one within the error bar for the number of hole generation less than five. Therefore, it is suggested that the observed hole generation follows the Poisson statistics as expected, and the proposed signal processing can properly extract the photon incidence information in real time. The large deviation of the experimental data from the theoretical one for larger number of hole generation (≥ 5) is probably due to the effect of the missing counts originating from the signals below the threshold level or higher count rate that cannot be resolved. Note that, for the smaller number of hole generation, the missing counts are partially compensated by the reduced λ that is obtained by the total counts divided by T_{total}.

In general, single-photon detectors based on elementary charge counting can be classified based on the lifetime of photogenerated charges. In the case of QD-gated FET[18] and Si-nanowire detector[19], the lifetime is relatively short, and output signal with adjacent rising and falling edges can be observed. In the case of CSIP[22] and QDOGFET[23),24], the lifetime is relatively long,

and staircase-like signal can be observed. The developed signal processor can handle both cases since it can only detect and measure the step height of the rising edges by focusing on the positive peaks in differential signal. Although the narrow bandwidth (800 Hz) of the preamplifier limits the MCR to 300 s^{-1} in the current setup[27], the processor can operate with thousand times higher clock frequency as described in Section 2, and thus cover wide range of applications by satisfying the target specification in Table I. The developed processor surely gives a large impact on expanding the usage of photodetectors based on elementary charge counting.

Summary

In order to process the complex output waveforms from the SOI MOSFET single-photon detector in real time, an FPGA-based signal processor has been developed. With this processor, the timing and the number of photogenerated holes are instantaneously analyzed, and also the counts in bins of the generated holes in a unit observation time are accumulated to verify the photon number statistics. It is successfully demonstrated that the obtained histogram of the photogenerated holes and the evolution of the event probability with respect to the light intensity follow the Poisson statistics, suggesting that the signal processor can properly extract the photon incidence information in real time. The results open up an opportunity for the wider use of the photon detectors based on elementary charge counting by providing the signal processor for their complex output waveforms. Since such a class of detectors feature wide spectral coverage, small DCR, excellent PNR and low-voltage operation, the scientific impact of this work is considerable.

References

1) L. Alaverdian, S. Alaverdian, O. Bilenko, I. Bogdanov, E. Filippova, D. Gavrilov, B. Gorbovitski, M. Gouzman, G. Gudkov, S. Domratchev, O. Kosobokova, N. Lifshitz, S. Luryi, V. Ruskovoloshin, A. Stepoukhovitch, M. Tcherevishnick, G. Tyshko, and V. Gorfinkel, Electrophoresis **23,** 2804 (2002).
2) B. L. Legendre, D. C. Williams, S. A. Soper, R. Erdmann, U. Ortmann, and J. Enderlein, Rev. Sci. Instrum. **67,** 3984 (1996).
3) C. Niclass, A. Rochas, P.-A. Besse, and E. Charbon, IEEE J. Solid-State Circuits **40,** 1847 (2005).
4) J. Kataoka, A. Kishimoto, T. Fujita, T. Nishiyama, Y. Kurei, T. Tsujikawa, T. Oshima, T. Taya, Y. Iwamoto, H. Ogata, H. Okochi, S. Ohsuka, H. Ikeda, and S. Yamamoto, Nucl. Instrum. Methods Phys. Res. Sect. A **784**, 248 (2015).
5) N. Gisin, G. Ribordy, W. Tittel, and H. Zbinden, Rev. Mod. Phys. **74,** 145 (2002).
6) H. Kosaka, A. Tomita, Y. Nambu, T. Kimura, and K. Nakamura, Electron. Lett. **39,** 1199 (2003).
7) A. Beveratos, R. Brouri, T. Gacoin, A. Villing, J. -P. Poizat, and P. Grangier, Phys. Rev. Lett. **89,** 187901 (2002).
8) A. L. Lacaita, P. A. Francese, and S. D. Cova, Opt. Lett. **18,** 1110 (1993).
9) W. Becker, A. Bergmann, M. A. Hink, K. Konig, K. Benndorf, and C. Biskup, Microsc. Res. Tech. **63,** 58 (2004).
10) D. M. Grant, J. McGinty, E. J. McGhee, T. D. Bunney, D. M. Owen, C. B. Talbot, W. Zhang, S. Kumar, I. Munro, P. M. P. Lanigan, G. T. Kennedy, C. Dunsby, A. I. Magee, P. Courtney, M. Katan, M. A. A. Neil, and P. M. W. French, Opt. Express **15,** 15656 (2007).
11) M. H. Devoret and R. J. Schoelkopf, Nature **406**, 1039 (2000).

12) K. Nishiguchi, C. Koechlin, Y. Ono, A. Fujiwara, H. Inokawa, and H. Yamaguchi, Jpn. J. Appl. Phys. **47**, 8305 (2008).
13) A. N. Cleland, D. Esteve, C. Urbina, and M. H. Devoret, Appl. Phys. Lett. **61,** 2820 (1992).
14) S. Komiyama, O. Astafiev, V. Antonov, T. Kutsuwa, and H. Hirai, Nature **403,** 405 (2000).
15) O. Astafiev, S. Komiyama, T. Kutsuwa, V. Antonov, Y. Kawaguchi, and K. Hirakawa, Appl. Phys. Lett. **80,** 4250 (2002).
16) R. Nuryadi, Y. Ishikawa, and M. Tabe, Phys. Rev. B **73,** 045310 (2006).
17) A. J. Shields, M. P. O'Sullivan, I. Farrer, D. A. Ritchie, R. A. Hogg, M. L. Leadbeater, C. E. Norman, and M. Pepper, Appl. Phys. Lett. **76,** 3673 (2000).
18) B. E. Kardynał, S. S. Hees, A. J. Shields, C. Nicoll, I. Farrer, and D. A. Ritchie, Appl. Phys. Lett. **90,** 181114 (2007).
19) A. Fujiwara, K. Yamazaki, and Y. Takahashi, Appl. Phys. Lett. **80,** 4567 (2002).
20) K. Nishiguchi, Y. Ono, A. Fujiwara, H. Yamaguchi, H. Inokawa, and Y. Takahashi, Appl. Phys. Lett. **90**, 223108 (2007).
21) Z. An, J.-C. Chen, T. Ueda, S. Komiyama, and K. Hirakawa, Appl. Phys. Lett. **86**, 172106 (2005).
22) T. Ueda, Z. An, K. Hirakawa, and S. Komiyama, J. Appl. Phys. **103,** 093109 (2008).
23) E. J. Gansen, M. A. Rowe, M. B. Greene, D. Rosenberg, T. E. Harvey, M. Y. Su, R. H. Hadfield, S. W. Nam, and R. P. Mirin, Nat. Photonics **1,** 585 (2007).
24) M. A. Rowe, G. M. Salley, E. J. Gansen, S. M. Etzel, S. W. Nam, and R. P. Mirin, J. Appl. Phys. **107,** 063110 (2010).
25) S. Pellegrini, R. E. Warburton, L. J. J. Tan, J. S. Ng, A. B. Krysa, K. Groom, J. P. R. David, S. Cova, M. J. Robertson, and G. S. Buller, IEEE J. Quantum Electron. **42,** 397 (2006).
26) Hamamatsu Photonics K.K., *Hamamatsu Photomultiplier Tubes - Basics and Applications* (Hamamatsu Photonics K.K. Electron Tube Division, 2007) 3rd ed., pp. 14-18.
27) W. Du, H. Inokawa, H. Satoh, and A. Ono, Opt. Lett. **36,** 2800 (2011).
28) W. Du, H. Inokawa, H. Satoh, and A. Ono, Jpn. J. Appl. Phys. **51,** 06FE01 (2012).
29) V. Singh, H. Inokawa, T. Endoh, and H. Satoh, Jpn. J. Appl. Phys. 49, 128002 (2010).
30) Preamplifier bandwidth is based on the experimental relationship between MCR and the bandwidth[27], preamplifier sensitivity is related to the bandwidth in view of the commercial product specifications by Analog Devices, Inc., the sampling and FPGA clock frequencies are the maximum values for the current FPGA and the circuit design. Note that the sampling frequency is well above the value required by the Nyquist theorem.
31) See Tecan Infinite 200 PRO as an example of microplate reader.
32) N. Nakata and T. Kamidate, Luminescence **16**, 263 (2001).
33) See Hamamatsu Photonics H10682-110 as an example of photon counting system with PMT.
34) A. Savitzky, and M. J. E. Golay, Anal. Chem. **36**, 1627 (1964).
35) Simulation environment consists of MATLAB (release R2012a), 64-bit Windows 10 Enterprise, Intel Core i7-4770 CPU @3.4 GHz and 8-GB memory.
36) Y. Sharma, H. Satoh, and H. Inokawa, IEICE Electron. Express **15,** 1 (2018).
37) SOPRALAB, N&K database [Online]. Available: http://www.sspectra.com/sopra.html
38) W. J. Thompson, Comput. Sci. Eng. **3,** 78 (2001).